Journal of
Materials Chemistry C

PAPER

View Article Online
View Journal | View Issue

Cite this: J. Mater. Chem. C, 2015, 3, 7022

Ultrahigh photo-responsivity and detectivity in multilayer InSe nanosheets phototransistors with broadband response†

Wei Feng,[ab] Jing-Bin Wu,[c] Xiaoli Li,[c] Wei Zheng,[a] Xin Zhou,[d] Kai Xiao,[e] Wenwu Cao,[f] Bin Yang,[f] Juan-Carlos Idrobo,[e] Leonardo Basile,[e] Weiquan Tian,[d] PingHeng Tan*[c] and PingAn Hu*[a]

Received 29th April 2015,
Accepted 15th May 2015

DOI: 10.1039/c5tc01208b

www.rsc.org/MaterialsC

We demonstrate the strategies and principles for the performance improvement of layered semiconductor based photodetectors using multilayer indium selenide (InSe) as the model material. It is discovered that multiple reflection interference at the interfaces in the phototransistor device leads to a thickness-dependent photo-response, which provides a guideline to improve the performance of layered semiconductor based phototransistors. The responsivity and detectivity of InSe nanosheet phototransistor can be adjustable using applied gate voltage. Our InSe nanosheet phototransistor exhibits ultrahigh responsivity and detectivity. An ultrahigh external photo-responsivity of $\sim 10^4$ A W^{-1} can be achieved from broad spectra ranging from UV to near infrared wavelength using our InSe nanosheet photodetectors. The detectivity of multilayer InSe devices is $\sim 10^{12}$ to 10^{13} Jones, which surpasses that of the currently exploited InGaAs photodetectors (10^{11} to 10^{12} Jones). This research shows that multilayer InSe nanosheets are promising materials for high performance photodetectors.

Introduction

Broadband sensing from the ultraviolet (UV)-visible to the near infrared (NIR) wavelength has various applications in image sensing, communications, environmental monitoring, and remote control.[1–5] Traditionally, separate sensors or materials are used for different sub-bands in the range from UV to NIR wavelength.[1–3] For example, gallium nitride (GaN), silicon (Si) and indium-gallium-arsenide (InGaAs) are commonly used for sensing UV, visible and NIR light, respectively.[4,5] The photo-responsivity of GaN and –Si based photodetectors is below 0.2 A W^{-1}, and the responsivity of InGaAs devices is usually less than 1 A W^{-1}.[4,5] The detectivity of silicon photodetectors is $\sim 4 \times 10^{12}$ Jones (1 Jones = 1 cm $Hz^{1/2}$ W^{-1}), and a typical detectivity of InGaAs is greater than 10^{12} Jones when it is cooled down to 4.2 K.[4,5] It would be greatly advantageous to have a broadband photodetector system with high sensitivity, fast speed, wide spectral response from UV to NIR, and high detectivities achievable at room temperature.

A small band-gap semiconducting polymer blended with a fullerene derivative was used to fabricate high detectivity photodetectors with a wide spectral response from UV to NIR. This polymer photodetector exhibited a high detectivity greater than 10^{12} Jones at room temperature, but a low photo-responsivity of only 0.17 A W^{-1}.[6] PbS colloidal quantum dots were exploited to give a broadband response ranging from UV to NIR, exhibiting an ultrahigh responsivity of $>10^3$ A W^{-1} and a high detectivity of 1.8×10^{13} Jones at a wavelength of 1.3 μm at room temperature.[7] However, the lateral structure adopted in these PbS quantum dot photodetectors leads to a large driving voltage of ~ 100 V and a slow response, which limit their practical applications.

Recently, two-dimensional (2D) layered semiconductors such as transition-metal chalogenides (*e.g.* MoS_2, WS_2, GaS, and GaSe) have demonstrated attractive capabilities for optoelectronics due to their ultrathin thickness, atomic flatness and the facile manipulation as well as their tunable optical properties controlled by thickness.[8–15] These 2D ultrathin materials are usually obtained by "Scotch-tape" mechanical exfoliation, in

[a] Key Lab of Microsystem and Microstructure of Ministry of Education, Harbin Institute of Technology, No. 2 Yi Kuang Street, Harbin, 150080, China. E-mail: hupa@hit.edu.cn
[b] School of Materials Science and Engineering, Harbin Institute of Technology, Harbin, 150080, China
[c] State Key Laboratory of Super lattices and Microstructures, Institute of Semiconductors, Chinese Academy of Sciences, Beijing 100083, China
[d] State Key Laboratory of Urban Water Resource and Environment, Harbin Institute of Technology, Harbin, 150080, People's Republic of China
[e] Center for Nano phase Materials Sciences, Oak Ridge National Laboratory, One Bethel Valley Road, Oak Ridge, TN 37831, USA
[f] Condensed Matter Science and Technology Institute, Harbin Institute of Technology, Harbin 150080, China

† Electronic supplementary information (ESI) available. See DOI: 10.1039/c5tc01208b

view of layered structures with the weak van der Waals interaction between adjacent layers. Compared to traditional semiconducting films such as silicon or III–V semiconductors, 2D layered materials have more ideal surfaces free of dangling bonds, which reduce surface roughness scattering (leading to high mobilities) and interface traps (resulting in low density of the interface state on the semiconductor–dielectric interface); atomic thickness of 2D layered films allows more efficient electrostatics by gate voltage; and 2D layered films exhibit intriguing physical behaviour strongly dependent on the layer number (thickness), such as the band-gap structure transition of MoS_2 from an indirect structure in the bulk to a direct one in the monolayer. These unique features make 2D semiconductor nanosheets a new class of materials with superior properties, which are key to applications in electronics and optoelectronics. Recently, new optoelectronic devices have been demonstrated using various 2D nanosheets.[8,14–20] Single-layer or multilayer MoS_2-based photodetectors have a tunable spectral photoresponse[10,17] and are ultrasensitive to visible light, with photoresponsivities reaching as high as 880 A W^{-1}.[17] However, an ultralow response time ($\sim$4 s) hinders its practical application. UV-visible photodetectors based on few-layer GaSe and GaS nanosheets exhibit responsivities of 2.8 A W^{-1} and 19.2 A W^{-1}, respectively.[14,15] A low photoresponse of 34.7 mA W^{-1} was measured in few-layer InSe.[16] And UV-near IR photodetectors based on multilayer InSe[18] and In_2Se_3[19] show high responsivities of 12.3 A W^{-1} and 395 A W^{-1}, respectively. Also, multilayer GaTe photodetectors have been demonstrated to have a very high photoresponsivity of 10^4 A W^{-1} for UV-visible light.[20] It is still challenging to make phototransistors with both ultrahigh photoresponsivity and detectivity, and having a broadband spectra response. Especially, there are few reports about the thickness dependent photo-response in 2D layered semiconductors, which is a key issue in the devices constructed using ultrathin layered materials.

Here, we demonstrate broadband, ultrahigh responsivity multilayer InSe nanosheet phototransistors, which have a wide spectral response ranging from UV to NIR light. Our results confirm that multiple reflection interference at the interfaces in the air/InSe/SiO_2/Si multilayer configuration leads to the thickness-dependent photo-response, which provides a useful guideline to improve the performance of layered semiconductor phototransistors. The performance (responsivity and detectivity) of multilayer InSe nanosheet phototransistors can be efficiently tuned by applying gate voltage. Maximum external photoresponsivities of 5.6×10^4 A W^{-1} at the UV wavelength of 254 nm, 3×10^4 A W^{-1} at the visible light of 700 nm and 2×10^3 A W^{-1} at the NIR light of 850 nm have been achieved using InSe nanosheet phototransistors. At room temperature, the detectivity of InSe nanosheet phototransistors is 2×10^{13} Jones at the UV-visible band and 10^{12} Jones at the NIR band, which greatly surpass those of silicon photodetectors. Furthermore, these InSe devices exhibit a fast response time of $\sim$5 ms. The superior performances in InSe nanosheet photodetectors are mainly owing to high surface ratio, high carrier mobility combined with narrow bandgap and direct band structures.

Experimental

Synthesis and characterization of InSe nanosheets:

The bulk InSe crystal was prepared by using the modified Bridgman method. Multilayer InSe nanosheets were mechanically exfoliated from bulk InSe crystals and transferred onto the silicon substrate coated with 285 nm SiO_2. The thickness was determined by using atomic force microscopy (AFM, Nanoscope IIIa Vecco). The structure and composition of multilayer InSe nanosheets were identified by X-ray diffraction (XRD, Diffractometer-6000 with Cu Ka radiation (λ = 0.1542 nm)) and transmission electron microscopy (Tacnai-G2 F30, an accelerating voltage of 300 kV) coupled with energy-dispersion X-ray spectroscopy (EDS).

Fabrication of InSe FETs and photodetectors

The multilayer InSe nanosheets were transferred to the SiO_2/Si substrates. Cr/Au electrodes with 5 nm thick Cr and 35 nm thick Au were fabricated using a shadow mask. The transistor based Si/SiO_2 substrates were annealed at 200 °C for 30 min with 100 sccm Ar : H_2 (v/v = 9/1) to reduce the resistance and improve the contact for the devices.

Characterization of electronic and optoelectronic properties

Electrical characterization of transistors based on InSe nanosheet devices was performed by using a semiconductor characterization system (Keithley 4200 SCS) with a Lakeshore probe station. Mono-chromatic light of 254–850 nm was obtained by using optical filters using a 500 W xenon lamp as the light source. The photocurrent measurements were performed using a semiconductor characterization system (Keithley 4200 SCS) with a Lakeshore probe station. The intensities of the incident light source were identified using a power and energy meter (Model 372, Scienteck).

Results and discussion

InSe is a highly promising material for applications in optoelectronics, radiation detectors and solar energy conversion devices due to its small direct band-gap of 1.26 eV at room temperature.[21–25] InSe crystals in this study were synthesized by using elemental indium and selenide as precursors (detailed in the Experimental section). The crystalline structure of the as-prepared crystal is the β-type determined by X-ray diffraction (XRD) (Fig. S1, ESI†) measurements. β-InSe is composed of vertically stacked Se–In–In–Se sheets with weak bonding between adjacent sheets *via* the van der Waals force. Fig. 1a shows the crystal structure of the β-InSe sheet with a thickness of 6.2 Å and a top view of the InSe single sheet crystal structure, which is typically hexagonal. Fig. 1b presents a low magnification TEM image of InSe nanosheets with an inset of the selected area electron diffraction pattern (SEAD) providing another evidence for the formation of single crystalline β-InSe flakes with an orientation along the [100] zone axis. Fig. 1c shows an atomic-resolution scanning transmission electron microscopy (AR-STEM) image, which shows an ideal hexagonal lattice structure, with a lattice

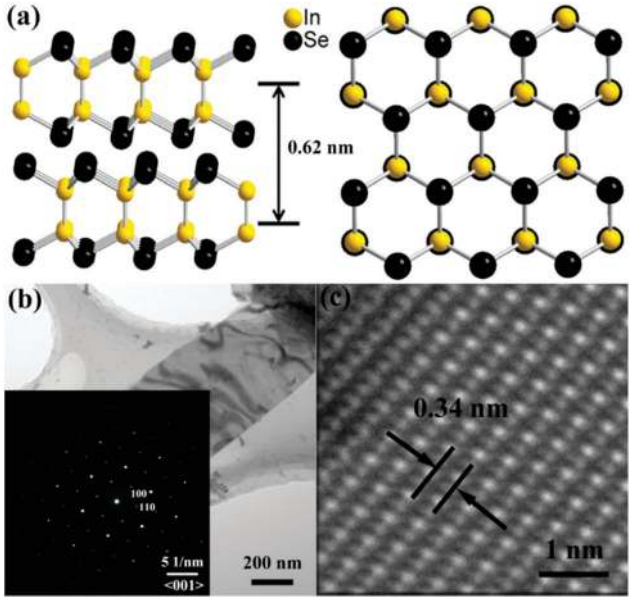

Fig. 1 Crystal structure and characterization of InSe nanosheets. (a) Crystal structure of InSe, the left part is the side view and the right part is the top view; (b) TEM images of multilayer InSe at low magnification; inset: the corresponding SAED pattern; and (c) the z-contrast STEM image showing the atomic structure of InSe nanosheets.

spacing of 0.34 nm, corresponding to the lattice constant of the (100) direction. The In/Se atomic ratio was calculated to be 1 : 1 by energy-dispersive X-ray spectroscopy (EDS) (Fig. S2, ESI†). Multilayer InSe nanosheets can be exfoliated from a bulk crystal and transferred to SiO_2/Si substrates.

Photon absorption is a very important physical process that determines the performance of layered material based photodetectors. We performed the theoretical simulations of light absorption inside InSe nanosheets lying on SiO_2/Si substrates as a function of the thickness, where the SiO_2 thickness is 285 nm. The absorption is determined by multiple reflection interference at the interfaces and in the interlayers and the complex refractive indices of each medium in the multilayer configuration. The multilayer optical interference method[26,27] has been widely used to quantify the optical contrast[27,28] and the Raman intensities[26,29–32] of ultrathin flakes of 2D crystals. Here, we adopt this method to study photon absorption of InSe nanosheets deposited on the SiO_2/Si substrate when the light is vertically incident onto the InSe nanosheets.

A multilayer configuration, air/InSe/SiO_2/Si, is proposed as shown in Fig. 2a, where air, InSe, SiO_2 and Si layers are, respectively, denoted by indices i = 0, 1, 2, and 3. The corresponding thickness and complex refractive indices are designated by d_i and $\check{n}_i(\lambda) = n_i(\lambda) - ik_i(\lambda)$, where the n_i and k_i values are functions of wavelength (λ) for InSe,[33] SiO_2[34] and Si.[34] The total photon absorption in the whole InSe layer can be expressed as:

$$\gamma_{ab} \propto \int_0^{d_1} \beta\left(|F_{ab}(Z)|^2\right) dZ$$

where $\beta = 4\pi k_1/\lambda$ is the absorption coefficient of bulk InSe, F_{ab} is the enhancement factor due to the multilayer optical

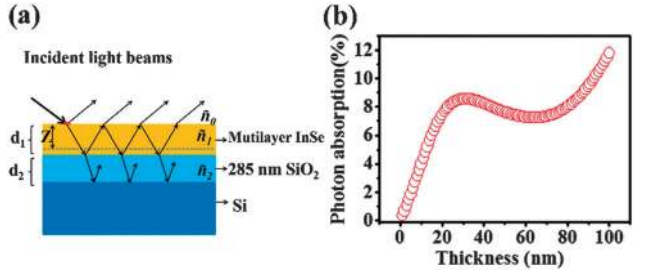

Fig. 2 (a) Schematic of the photon absorption of the InSe multilayer on the SiO_2/Si substrate; (b) thickness-dependent photo absorption.

interference effect, following the notation reported by Duhee Yoon[26] and Naeyoung Jung.[30] In the calculations, the electric field amplitude of the incident photons has been normalized, so $F_{ab}(Z)$ denotes the electric field amplitude of the incident photons at depth Z in the InSe layer.[29,32] For convenience, we calculated $F_{ab}(Z)$ by means of the transfer matrix method.[27,28,31] Then, we can get the total photon absorption in the whole InSe layer with a thickness of d_1. By integrating over the InSe thickness, as represented by the above equation. As an example, Fig. 2b shows the total photon absorption of the InSe flakes dependent on the thickness in a range of 1–100 nm when the photon wavelength is set to 700 nm. The total photon absorption exhibits a peak around the thickness of 30 nm, which means that there exists an optimized thickness of the InSe layer for application in photon detectors. The theoretical simulations of light absorption of InSe nanosheets deposited on the SiO_2/Si substrate suggests that 30–40 nm InSe nanosheets are optimal channels for high performance photodetectors because of the direct band-gap and best phonon absorption.

InSe field effect transistors (FETs) and phototransistors are fabricated using Cr/Au contacts on 285 nm SiO_2/Si substrates. Fig. 3a describes the schematic structure of the device in this study. Electrical properties and optoelectronic characterization are measured with a back gate structure at room temperature under ambient conditions. The thickness of InSe nanosheets is in the range of 4–60 nm, which is measured by atomic force microscopy (AFM).

The fabricated multilayer InSe FETs (Fig. 3b, channel length ~20 μm; width ~15 μm, and Fig. S3 (ESI†): thickness of the channel ~30 nm) shows typical n-type FET properties (Fig. 3c and d). The I_{ds}–V_{ds} characteristics agree with the conventional long-channel n-type MOS transistor, showing a linear regime at low V_{ds} and a saturation regime at high V_{ds}. This feature is an important factor for practical applications since thin film transistors (TFTs) in organic light emitting diode (OLED) displays are working in the saturation current region. InSe FETs show the saturation of drain current because the conducting channel is converted to the "pinch-off" condition at high V_{ds}. The current on/off ratio is calculated by adopting the ratio of maximum to minimum I_{ds} from the plot of V_g *vs.* I_{ds}. The current on/off ratio is 10^7 for this device. The mobility of multilayer InSe transistors can be extracted using the equation $\mu = [L/(W \times (\varepsilon_0\varepsilon_r/d) \times V_{ds})] \times dI_{ds}/dV_g$, where L = 20 μm is the length of the transistor, W = 15 μm is the width of the

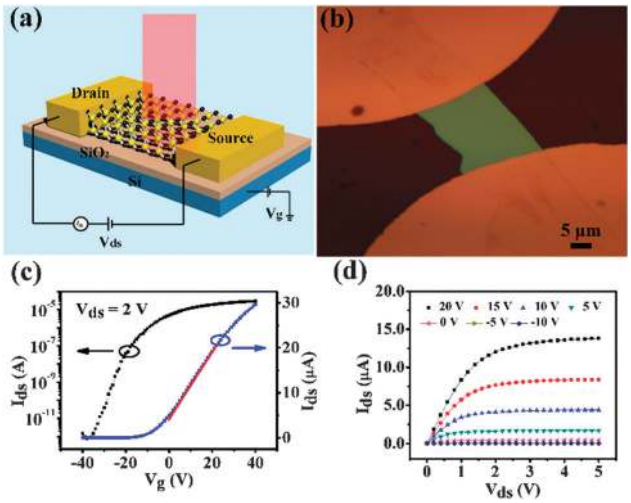

Fig. 3 Multilayer InSe nanosheet transistor and phototransistor. (a) Schematic drawing of a phototransistor based on InSe nanosheets; (b) a typical image of the InSe nanosheets; (c) a typical transfer curve of the InSe nanosheet transistor; and (d) the corresponding output curve of InSe nanosheet transistors.

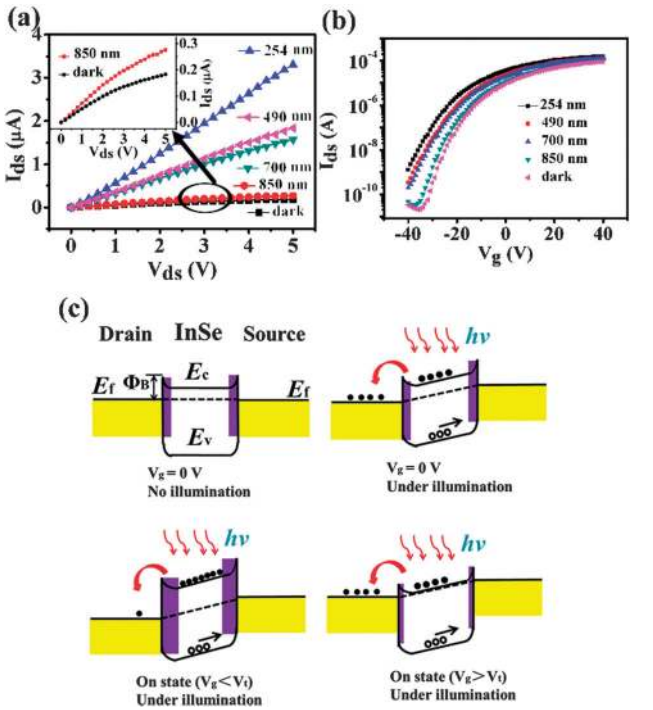

Fig. 4 Photoinduced response of the multilayer InSe nanosheet phototransistor. (a) Drain–source (I_{ds}–V_{ds}) characteristics of the device at V_g = 0 V and under different illumination wavelengths with a light intensity of 0.29 mW cm^{-2}; the inset is enlarged phototcurrrent under 850 nm illumination. (b) Gating response (I_{ds}–V_g) of the InSe phototransistor in the dark and under the illumiation of 254 nm, 490 nm,700 nm and 850 nm light with an intensity of 0.29 mW cm^{-2} at V_{ds} = 5 V. (c) The band digaram of the InSe nanosheet phototransistor: E_F is the Fermi level energy, E_c the minimum conduction band energy, E_v the maximum valence band energy and Φ_B the barrier height.

transistor, $\varepsilon_0 = 8.854 \times 10^{-12}$ Fm^{-1} is the vacuum permittivity, ε_r is 3.9 for SiO_2 and d (285 nm) is the thickness of SiO_2. The mobility of the transistor is calculated to be 32.6 cm^2 V^{-1} s^{-1} in the ambient environment (Fig. 3c, V_{ds} = 2 V). High carrier mobility can promote the photocurrent inside the multilayer InSe nanosheet device.

To measure the photoresponse of multilayer InSe nanosheet devices on SiO_2/Si substrates, monochromatic light illumination was directed vertically onto devices consisting of two Cr/Au electrodes and InSe nanosheet channels with 20 μm being the length and 15 μm being the width (depicted in Fig. 3). Optoelectronic characterization was recorded with a fixed illumination intensity of 0.29 mW cm^{-2} under different illumination wavelengths ranging from 254 nm to 850 nm (Fig. 4a and b). The device shows a broad spectral response to light from the ultraviolet to the near infrared regions. The I_{ds}–V_{ds} curves shown in Fig. 4a exhibit a significant increase of source–drain current by one order of magnitude as the device is illuminated. Accordingly, the photocurrents I_{ph} ($I_{ph} = I_{illumination} - I_{dark}$) also increase with the bias voltage V_{ds}, which is due to the increase in carrier drift velocity and the related decrease of carrier transit time T_t.

The dependence of photocurrent on the gate bias was investigated under illumination of 254 nm, 490 nm, 700 nm and 850 nm light with a fixed illumination intensity of 0.29 mW cm^{-2} and a bias voltage of 5 V (shown in Fig. 4b). The ratio of photocurrents at the ON state *versus* OFF state can reach an order of 10^6, so that the photocurrent flowing through the whole circuit is efficiently controlled by applying gate voltage. In both OFF and ON states the device current increases across the whole gate voltage range employed. This indicates that the photocurrent dominates over thermionic and tunnelling currents across the entire operating range of gate voltages.

The observed gate dependent behaviour of multilayer InSe nanosheet phototransistors can be explained using a simple energy band diagram (Fig. 4c). When metal electrodes come in contact with InSe nanosheets, a charge transfer occurs at the interfaces *via* Femi level tuning at an equilibrium, which causes the accumulation of space charges in the contact region together with a band bending to form Schottky type barriers as well as a depletion layer. As the OFF state devices are illuminated ($V_g < V_t$), light absorption and excitations of hole–electron pairs occur, which can be extracted to generate photocurrent by applying a bias. The photocurrent increases with decreasing wavelength because the higher excitation energy provided by higher photon energies can produce more excitations. In the ON state ($V_g > V_t$), photo-excited current and the thermionic, tunnelling currents all contribute to the device current. Increasing gate voltage can shift down the band and decrease the depletion layer to lower the barrier heights at contacts, resulting in more efficient photocurrent extraction and an enhanced photoresponse.

Responsivity (R_λ) is a critical parameter to evaluate the performance of a phototransistor. The R_λ is defined as the photocurrent generated per unit power of the incident light on the effective area of a phototransistor[20] The R_λ value can be calculated by the following equation: $R_\lambda = I_\lambda/P_\lambda S$. Here, I_λ is the generated photocurrent, P_λ is the incident light intensity,

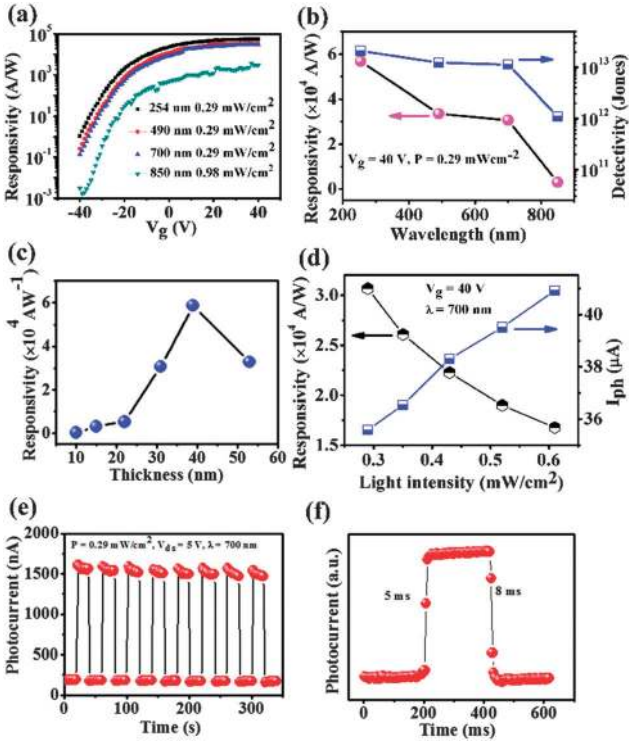

Fig. 5 Photoresponse performance of the multilayer InSe phototransistor. (a) Gate voltage dependent responsivity under a bias voltage V_{ds} = 2 V and light intensity P = 0.29 mW cm^{-1} under the illumination of light with wavelengths of 254 nm, 490 nm, 700 nm and 850 nm; (b) responsivity and detectivity as a function of illumination wavelengths with light intensity P = 0.29 mW cm^{-1} at the gate bias V_g = 40 V; (c) responsivity as a function of InSe thickness; (d) responsivity and photocurrent as a function of illumination intensity under a wavelength of 700 nm at the gate bias V_g = 40 V (e), (f) time-resolved photoresponse of the InSe photodetector under the illumination of 700 nm light with the voltage V_{ds} = 5 V and light intensity P = 0.29 mW cm^{-1}.

S (300 μm^2) is the effective illuminated area. Fig. 5a shows gate dependent responsivity (R_λ) acquired at bias voltage V_{ds} = 5 V. Responsivity is also highly tunable by the applied gate voltage (shown in Fig. 5a). For example, the responsivity measured under the illumination of 254 nm (R_{245nm}) increases from 1.65 × 10^{-3} A W^{-1} at V_g = −40 V (OFF state) to 2.31 × 10^4 A W^{-1} at V_g = 0, and to 5.68 × 10^4 A W^{-1} at V_g = 40 V (ON state). Our InSe nanosheet phototransistors are super-responsive to a broad spectral range from UV-visible to NIR, as shown in Fig. 5b. The responsivity measured under broadband illumination of ultraviolet (254 nm), visible (490 nm and 700 nm) and near infrared light (850 nm) are R_{254nm} = 5.68 × 10^4 A W^{-1}, R_{490nm} = 3.574 × 10^4 A W^{-1}, R_{700nm} = 3.06 × 10^4 A W^{-1} and R_{850nm} = 2.975 × 10^3 A W^{-1}, respectively. The responsivities of our multilayer InSe nanosheet photodetectors much higher than those of the currently used silicon or InGaAs photodetector (<2 A W^{-1}) even largely surpass all presently reported values for other 2D layered material based optoelectronics[8,14–20] (see more information in Table S1, ESI†).

Another important parameter to evaluate the performance of photodetectors is the specific detectivity (D^*). The normalized detectivity D^* is measured in units of Jones (cm Hz$^{1/2}$ W^{-1}). D^* is given as $(A\Delta f)^{1/2}R$/in, where A is the effective area of the detector in cm^2, Δf is the electrical bandwidth in Hz, and R is the responsivity in A W^{-1} measured under the same conditions as the noise current (in Amperes). The material figure of merit D^* allows comparison among devices of different areas and geometries. There are three contributions to the total noise that limit D^*: shot noise from dark current, Johnson noise, and thermal fluctuation noise. The shot noise from the dark current is the major contributor to the total noise in this case; the detectivity can be calculated by the equation: $D^* = RA^{1/2}/(2eI_d)^{1/2}$, where R is responsivity, A is the area of the phototransistor channel, e is the electron charge, and I_d is the dark current.[3] Fig. 5b shows the calculated D^* of a phototransistor at different wavelengths. The D^* is ∼10^{13} Jones in the visible light and the ultraviolet region and ∼10^{12} Jones in the NIR region, which both surpass the D^* values of the currently used Si or InGaAs photodetectors (∼10^{11}–10^{12} Jones),[4,5] and MoS_2 and In_2Se_3 devices (∼10^{11} to 10^{12} Jones).[17,19]

The theoretical simulations of light absorption of InSe nanosheets deposited on the SiO_2/Si substrate indicate that the thickness is a crucial element for achieving high performance of photodetectors. Fig. 5c shows the responsivity as a function of thickness, which was measured with 700 nm light illumination at a light intensity of 0.29 mW cm^{-2} under a bias of 5 V. The photoresponse increases from 10 nm to 40 nm and then starts to decrease with thickness. The responsivity is proportion to the photocurrent, and the photocurrent is mainly dependent on light absorption. Theoretical simulation shows that there is a peak between 30–40 nm for light absorption of InSe nanosheets. The experimental results can be explained by former simulation. The maximum photoresponse is achieved at a thickness of about 40 nm, whereas maximum photon-adsorption was obtained at ∼30 nm (shown in Fig. 2c). Photocurrent generation consists of photon-adsorption, photo-carrier generation and the photocurrent generation through extraction and transport. Actually, a 30 nm thick InSe sheet shows an adsorption of 8.96%, which is a little different from that of 40 nm InSe with an adsorption of 7.91%. At almost the same photo-adsorption rate, other factors (photo-carrier generation or photo-carrier transport) influenced by the thickness will further modify the optimized thickness, which need to be further investigated.

When the photon energy is higher than the E_g of InSe, the generated photocurrent is controlled by the illuminated intensity. Fig. 5d shows I_{ph} as a function of illumination intensity under 700 nm at the gate bias V_g = 40 V. The generated I_{ph} increase gradually with the light intensity increasing from 0.29 mW cm^{-2} to 0.61 mW cm^{-2}. In other words, multilayer InSe phototransistors can generate a light intensity dependent I_{ph}. The good linearity between I_{ph} and light intensity confirms that the generated photocurrent is determined by the quantity of photogenerated carriers under illumination. As the illumination intensity is increased, the responsivity is degraded, which is due to the trap states existing in InSe or at the interface between InSe and the dielectric substrate.

The response speed is another important parameter of photodetectors. The temporal response of our multilayer InSe nanosheet phototransistors was characterized using a chopper generated short light pulse. Fig. 5e and f show the transient photocurrent of our InSe nanosheet device measured under a bias of 5 V at a light intensity of 0.29 mW cm^{-2}. With the light irradiation at 700 nm on and off, our InSe nanosheet photodetectors exhibit a repeatable and stable response to incident light. The response time is calculated by averaging the duration values between light-ON and light-OFF (corresponding to 80% increase or decay). The measured rise and fall time are 5 ms and 8 ms, respectively, which are much faster than that of single-layer MoS_2 devices (response time: 50 ms).[8]

Conclusions

In summary, we have demonstrated multilayer InSe nanosheet transistors and phototransistors. The photon adsorption inside InSe nanosheets exhibits a strong dependence on the thickness, which is originated from multiple reflection interference at the interfaces of the air/InSe/SiO_2/Si multilayer configuration. The multilayer InSe transistors show an intrinsic n-type semiconductor conductance and exhibit a high mobility of 32 cm^2 V^{-1} s^{-1} and a high current on/off ratio $\sim 10^7$. The multilayer InSe nanosheet phototransistors have a broad spectral response from UV to NIR light. The performance (photoresponsivity, detectivity) of multilayer InSe nanosheet phototransistors can be efficiently controlled by the applied gate voltage. Maximum external photoresponsivities of 5.6×10^4 A W^{-1} at the UV wavelength of 254 nm, 3×10^4 A W^{-1} at the visible light wavelength of 700 nm and 2×10^3 A W^{-1} at the NIR light wavelength of 850 nm have been achieved. At room temperature, the detectivities of InSe nanosheet photodetectors are 2×10^{13} Jones at the UV-visible wavelength, and $\sim 10^{12}$ Jones at NIR. The performance parameters of our phototransistors greatly surpass that of the currently used silicon photodetectors[4,5] and other reported photodetectors based on layered materials.[14–20] These ultrahigh performances of our multilayer InSe nanosheet phototransistors are mainly owing to high carrier mobility, narrow bandgap and direct band structures of InSe nanosheets. Such high performances make multilayer InSe nanosheet phototransistors very attractive for various applications in touch sensors panels, image sensors and solar cells.

Acknowledgements

This work is supported by National Natural Science Foundation of China (NSFC, No. 61172001, 21373068, 11225421, 11434010 and 11474277), the National Key Basic Research Program of China (973 Program) under Grant No. 2013CB632900; A portion of this research was conducted at the Center for Nanophase Materials Sciences, which is a DOE office of Science User Facility.

Notes and references

1 A. Rogalski, J. Antoszewski and L. Faraone, *J. Appl. Phys.*, 2009, **105**, 091101.
2 M. Ettenberg, *Adv. Imaging*, 2005, **20**, 29–32.
3 E. H. Sargent, *Adv. Mater.*, 2005, **17**, 515–522.
4 E. Monroy, F. Omnès and F. Calle, *Semicond. Sci. Technol.*, 2003, **8**, R33.
5 R.-H. Yuang, J.-I. Chyi, W. Lin and Y.-K. Tu, *Opt. Quantum Electron.*, 1996, **28**, 1327–1334.
6 X. Gong, M. Tong, Y. Xia, W. Cai, J. S. Moon, Y. Cao, G. Yu, C.-L. Shieh, B. Nilsson and A. J. Heeger, *Science*, 2009, **325**, 1665–1667.
7 G. Konstantatos, I. Howard, A. Fischer, S. Hoogland, J. Clifford, E. Klem, L. Levina and E. H. Sargent, *Nature*, 2006, **442**, 180–183.
8 Z. Yin, H. Li, H. Li, L. Jiang, Y. Shi, Y. Sun, G. Lu, Q. Zhang, X. Chen and H. Zhang, *ACS Nano*, 2012, **6**, 74–80.
9 Y. Zhang, Y. Zhang, Q. Ji, J. Ju, H. Yuan, J. Shi, T. Gao, D. Ma, M. Liu, Y. Chen, X. Song, H. Y. Hwang, Y. Cui and Z. Liu, *ACS Nano*, 2013, **7**, 8963–8971.
10 X. Huang, Z. Zeng and H. Zhang, *Chem. Soc. Rev.*, 2013, **42**, 1934–1946.
11 M. Chhowalla, H. S. Shin, G. Eda, L.-J. Li, K. P. Loh and H. Zhang, *Nat. Chem.*, 2013, **5**, 263–275.
12 Z. Zeng, Z. Yin, X. Huang, H. Li, Q. He, G. Lu, F. Boey and H. Zhang, *Angew. Chem., Int. Ed.*, 2011, **50**, 11093–11097.
13 Q. He, Z. Zeng, Z. Yin, H. Li, S. Wu, X. Huang and H. Zhang, *Small*, 2012, **8**, 2994–2999.
14 P. A. Hu, Z. Wen, L. Wang, P. Tan and K. Xiao, *ACS Nano*, 2012, **6**, 5988–5994.
15 P. A. Hu, L. Wang, M. Yoon, J. Zhang, W. Feng, X. Wang, Z. Wen, J. C. Idrobo, Y. Miyamoto, D. B. Geohegan and K. Xiao, *Nano Lett.*, 2013, **13**, 1649–1654.
16 S. Lei, L. Ge, S. Najmaei, A. George, R. Kappera, J. Lou, M. Chhowalla, H. Yamaguchi, G. Gupta, R. Vajtai, A. D. Mohite and P. M. Ajaya, *ACS Nano*, 2014, **8**, 1263–1272.
17 L. Sanchez, D. Lembke, M. Kayci, A. Radenovie and A. Kis, *Nat. Nanotechnol.*, 2013, **8**, 497–501.
18 T. R. Srinivasa, Y.-Y. Lu, R. K. U. R. Sankar, C.-D. Liao, C.-H. Cheng, F. C. Chou and Y.-T. Chen, *Nano Lett.*, 2014, **14**, 2800–2806.
19 R. B. Jacobs-Gedrim, M. Shanmugam, N. Jain, C. A. Durcan, M. T. Murphy, T. M. Murray, R. J. Matyi, R. L. Moore and B. Yu, *ACS Nano*, 2013, **8**, 514–521.
20 F. Liu, H. Shimotani, H. Shang, T. Kanagasekaran, V. Zlyómi, N. Drummond, V. I. FaI'ko and K. Tanigaki, *ACS Nano*, 2014, **8**, 752–760.
21 M. V. Andriyashik, M. Y. Sakhnovskii, V. B. Timofeev and A. S. Yakimova, *Phys. Status Solidi*, 1968, **28**, 277–285.
22 S. Gopal, C. Viswanathan, B. Karunagaran, S. K. Narayandass, D. Mangalaraj and J. Yi, *Cryst. Res. Technol.*, 2005, **40**, 557–567.
23 G. Micocci and A. Tepore, *Sol. Energy Mater.*, 1991, **22**, 215–222.
24 M. A. Kenawy, H. A. Zayed and A. M. A. El-Soud, *J. Mater. Sci.: Mater. Electron.*, 1990, **1**, 115–117.
25 M. M. El-Nahass, A.-B. A. Saleh, A. A. A. Darwish and M. H. Bahlol, *Opt. Commun.*, 2012, **285**, 1221–1224.

26 D. Yoon, H. Moon, Y.-W. Son, J. S. Choi, B. H. Park, Y. H. Cha, Y. D. Kim and H. Cheong, *Phys. Rev. B: Condens. Matter Mater. Phys.*, 2009, **80**, 125422.
27 C. Casiraghi, A. Hartschuh, E. Lidorikis, H. Qian, H. Harutyunyan, T. Gokus, K. S. Novoselov and A. C. Ferrari, *Nano Lett.*, 2007, **7**, 2711–2717.
28 W. P. Han, Y. M. Shi, X. L. Li, S. Q. Luo, Y. Lu and P. H. Tan, *Acta Phys. Sin.*, 2013, **62**, 110702.
29 S.-L. Li, H. Miyazaki, H. Song, H. Kuramochi, S. Nakaharaia and K. Tsukagoshi, *ACS Nano*, 2012, **6**, 7281–7288.
30 N. Jung, A. C. Crowther, N. Kim, P. Kim and L. Brus, *ACS Nano*, 2010, **4**, 7005–7013.
31 Y. K. Koh, M.-H. Bae, D. G. Cahill and E. Pop, *ACS Nano*, 2011, **5**, 269–274.
32 Y. Y. Wang, Z. H. Ni, Z. X. Shen, H. M. Wang and Y. H. Wu, *Appl. Phys. Lett.*, 2008, **92**, 043121.
33 X.-L. Li, X.-F. Qiao, W.-P. Han, Y. Lu, Q.-H. Tan, X.-L. Liu and P.-H. Tan, *Nanoscale*, 2015, **7**, 8135–8141.
34 E. D. Palik, *Handbook of Optical Constants of Solids*, Academic Press, New York, 1985.

